Supplementary Information

Engineering egg-shell structure of Ag/SiO$_2$ pellet catalyst for selective hydrogenation of dimethyl oxalate to methyl glycolate

Xiaofeng Xu [a], Xin Hu [b], Zuwei Luo [a], Yueqiang Cao [b,*], Yi-An Zhu [a], Wei Li [b],

Jinghong Zhou [a,*] and Xinggui Zhou [a]

[a] State Key Laboratory of Chemical Engineering, East China University of Science

and Technology, 130 Meilong Road, Shanghai 200237, China.

[b] School of Chemical Engineering, East China University of Science and Technology,

130 Meilong Road, Shanghai 200237, China.

* Corresponding authors: yqcao@ecust.edu.cn; jhzhou@ecust.edu.cn.

1. Experimental methods

1.1 Preparation of egg-shell-type Ag/SiO$_2$ catalysts

Spherical silica pellets (Qingdao Bangkai, d_{pellet}=2-3 mm, d_{pore}=9 nm, S_{BET}=548 m^2/g) were firstly calcined in 550 °C for 4 h and dried in 120 °C for 2 h, and then a certain amount of spherical silica pellets were soaked in n-undecane (Merck, > 99%) for 20 min. The soaked pellets were subsequently transferred into an oven to evaporate a part of the n-undecane at 120 °C to obtain partially dried silica spherical supports. The amount of n-undecane removed was carefully controlled by varying the evaporation time. The amount of removed n-undecane was determined by the difference in the weight of the pellets before and after drying. Subsequently, an aqueous solution of AgNO$_3$ (Sinopharm, >99%) with an equal volume to the removed n-undecane was impregnated onto the partially dried support. As a reference, the homogeneously impregnated catalyst was also prepared by impregnating AgNO$_3$ solution onto the silica pellets, which were the same as mentioned but without n-undecane soaking before impregnation. Finally, the impregnated precursors were dried at 120 °C for 2 h and calcined at 400 °C for 4 h.

1.2 Catalyst characterizations

Scanning transmission electron microscopy (STEM) characterization was performed using ThermoFisher Talos F200X (FETEM, 200 kV). High angle annular dark field (HAADF)-STEM images were recorded using a convergence semi-angle of 11 mrad, and inner- and outer collection angles of 59 and 200 mrad, respectively. The Ag concentration profile was carried out on a scanning electron microscopy (FEI Nova NanoSEM 450) equipped with an energy-dispersive Fissons Kevex X-ray spectrometer operating at 20 kV. N$_2$ physisorption measurements were carried out on a Micrometrics ASAP 2020 apparatus, and a specific surface area and pore volume analysis were performed using the Brunauer–Emmett–Teller (BET) and Barrett–Joyner–Halenda (BJH) methods, respectively. Actual loadings of Ag in all catalysts were determined with ion-coupled plasma optical emission spectroscopy (ICP-OES) on an Agilent 5100 spectrometer. The shell layer thickness and the cross-section of the catalyst were observed by optical microscopy. The catalyst pellet was cut open and the average size of the shell layer in the catalyst pellet was determined by counting at least 10 pellets.X-ray photoelectron spectroscopy (XPS) measurements were measured on the American Thermo ESCALAB 250Xi with Al Ka (hν = 1486.6 eV). X-ray diffraction (XRD) tests were carried out on a Bruker D8 Advance X-ray diffractometer. The XRD-spectrum was recorded using Cu Kα-radiation in the range 2θ = 10–80° (step size 0.02°).

For the H_2-TPD tests, about 100 mg of the sample was firstly pre-reduced under 100 mL/min of 10% H_2/Ar flow for 3 h at 350 °C, followed by purging with pure Ar for 2 h at 300 °C to remove any physically adsorbed impurities. After cooling down to 70 °C, the flow of H_2 was introduced until the saturated adsorption was reached. Then, pure Ar was flushed to remove the physically adsorbed H_2. Finally, the temperature was increased to 600 °C with a rate of 5 °C/min under pure Ar, and the desorbed hydrogen species were detected by TCD detector.

In situ FTIR spectra of DMO adsorbed on catalysts were obtained on a PerkinElmer Frontier spectrometer equipped with a transmission cell.[1, 2] Typically, about 20 mg of sample was pressed into a self-supporting wafer and placed into a transmission cell with NaCl window. Then, 5% H_2/Ar was introduced at 50 ml/min and the sample was reduced at 350∘ C for 3 h. After purging the cell with pure Ar for 1 h, the temperature was cooled down to 80 ∘C, and then a certain amount of DMO was bubbled with pure Ar into the cell for DMO adsorption. After 1 h of DMO adsorption, the sample was evacuated with a vacuum pump to remove the free gas DMO and physically adsorbed DMO from the sample surface. The FTIR spectra were collected at 220 ºC with a resolution of 4 cm^{-1} and an accumulation of 64 scans.

1.3 Catalytic evaluation

A fixed-bed tubular continuous flow reactor (32 mm inner diameter and 600 mm length), equipped with an on-line gas chromatography, was used to evaluate the catalytic performance of the pellet catalysts for DMO hydrogenation. Typically, 1.35 g of the catalyst was loaded in the middle of the tubular flow reactor. The catalyst was reduced at 350°C for 6 h at a flow rate of 100 mL/min of H_2. After cooling to 220 °C, the pressure was raised to 2.5 MPa, and the DMO dissolved in methanol (10 wt%) was pumped into a vaporizer at 200 °C. Subsequently, H_2 with 100 of H_2/DMO molar ratio was flowed into the tubular reactor. The outlet stream was sampled at 30 min intervals using an automated Valco 6-way and analyzed the composition using an on-line gas chromatograph (FULI GC9790 PLUS). The chromatographic detector was a flame ionization detector (FID) and the column was a DB-624 capillary column (30 m × 0.45 mm × 0.85 μm). DMO conversion and product selectivities were calculated as follows:

$$Conversion(\%) = \frac{n_{DMO,in} - n_{DMo,out}}{W_{DMO,in}} \times 100\%$$

(1)

$$Selectivity(\%) = \frac{n_{MG,MF,EG\ or\ ET}}{n_{DMO,in} - n_{DMO,out}} \times 100\%$$

(2)

2. Calculations for the TOF

The mass of catalyst for each appraisal was 1.35 g. The actual loading of catalyst was determined by ICP, and the average particle size of Ag particles was obtained by HAADF-STEM images statistics. The results are shown in **Table S1**.

Table S1. Physical properties of catalysts.

	E20	E40	E60	E80	H
Ag loading[a]/wt.%	4.6	4.5	4.5	4.6	4.7
Average particle size (d)[b]/%	3.9	6	6.4	8.2	8.7

[a] Metal loading was determined by ICP-OES.
[b] Statistics were obtained from HAADF-STEM images.

Assuming that the Ag particles of the catalyst are spherical, the dispersion of Ag can be estimated according to the equation Dispersion(D)=1.178/d.[3, 4] The results are shown in **Table S2**.

Table S2. Dispersion of Ag particles on different catalysts

Catalysts	E20	E40	E60	E80	H
D/%	26.28	27.56	26.90	27.56	26.90

The TOF was calculated as follow:

$$TOF = \frac{v_{DMO} \times x_{DMO}}{N_{Ag} \times D} \tag{3}$$

where v_{DMO} is the molar flow rate of DMO, x_{DMO} is the DMO conversion, N_{Ag} is the molar amount of Ag loaded in the catalyst, and D is the dispersion of Ag in the catalyst. The TOF calculated from Equation (1) are shown in **Table S3**.

Table S3. The TOF values for different catalysts at LHSV=1 h^{-1}

Catalysts	E20	E40	E60	E80	H
TOF (h^{-1})	64.73	66.73	66.78	58.73	57.47

Table S4.   DMO conversion at different LHSV.

LHSV (h^{-1})	0.5	0.75	1	1.25
E20	94.15%	91.35%	85.66%	78.35%
E40	95.73%	93.87%	90.60%	85.41%
E60	96.75%	92.04%	88.51%	83.88%
E80	94.37%	90.94%	81.51%	66.50%
H	94.73%	89.26%	79.56%	65.21%

Table S5. MG selectivity at different LHSV.

LHSV (h^{-1})	0.5	0.75	1	1.25
E20	74.23%	83.35%	91.37%	94.37%
E40	72.28%	82.10%	87.79%	93.85%
E60	71.37%	82.35%	88.91%	92.75%
E80	78.35%	84.07%	88.24%	90.13%
H	75.78%	83.18%	86.85%	90.11%

Table S6. Catalytic performance of various reported catalysts for selective hydrogenation of DMO to MG.

| Catalysts | Cu/Ag loading (wt%) | Reaction conditions | | | | Conv._DMO (%) | Selec._MG (%) | TOF (h^{-1}) | Ref. |
		LHSV (h^{-1})	Temperature (K)	Pressure (MPa)	H$_2$/DMO (mol/mol)				
Cu-Ni/HMS[5]	2.6	0.2	493	2.5	100	100	86.0	10.6	[5]
Raney Cu[6]	100	2.0	483	2.5	100	70.0	95.0	4.2	[6]
Cu/HAP[7]	20.0	0.4	483	2.5	150	74.0	70.0	14.4	[7]
Cu/AC[8]	20.0	0.2	493	2.5	120	83.0	92.0	17.0	[8]
Cu/SiO$_2$[9]	48.5	0.26	493	2.5	200	>90.0	94.0	5.08	[9]
Cu-Ag/Ni-foam[10]	28.0/0.4	0.25	483	2.5	300	96.1	96.1	N/A	[10]
Ag/Ti-KCC-1[11]	10.3	1.75	473	3.0	100	98.0	95.0	16.1	[11]
Ag-B$_2$O$_3$/SiO$_2$[12]	10.0	0.2	453	0.5	150	98.9	97.2	N/A	[12]
Ag/AC-N[13]	9.8	0.6	493	3.0	80	95.0	98.0	25.1	[13]
Ag-in/h-CNT[14]	8.1	0.6	493	3.0	80	100	97.0	N/A	[14]
Ag-Ni/SBA-15[4, 15]	5.0	1.0	473	3.0	80	97.6	92.8	106.0	[4, 15]
Ag/KCC-1[16]	15.7	1.75	473	3.0	100	100	>90.0	53.2	[16]
Ag/SBA-15[17]	9.3	0.6	473	3.0	80	100	94.0	34.0	[17]
Ag/MCM-41[18]	10.0	0.2	493	2.5	100	96.0	94.0	1.9	[18]
Ag-SiO$_2$	4.5	1	493	2.5	100	90.60	87.79	66.73	This work

3. Calculations for the effectiveness factor

Internal diffusion occurs inside the catalyst pore and is normally composed of intermolecular diffusion and Knudsen diffusion, which can be described by the so-called "Dust-Gas" model.[19, 20] The Chapman-Enskog formula can be used to calculate the intermolecular diffusion coefficient with the following equation.[21]

$$D_{AB} = 0.0018583 \frac{T^{\frac{3}{2}}(1/M_A + 1/M_B)^{1/2}}{P_t \sigma_{AB}^2 \Omega_{AB}} \tag{4}$$

where, D_{AB} is molecular diffusion coefficient, cm²/s; T is temperature, K; M_A, M_B are molecular weight of gases A and B, respectively; P_t is total pressure of gas mixture, atm; σ_{AB} is molecular spacing corresponding to the Lennard-Jones potential energy function ε_{AB} for the molecular pair A-B, nm; Ω_{AB} is collision integral whose value is 1 for hard sphere molecules and $k_B T/\varepsilon_{AB}$ for real gases.

The Knudsen diffusion coefficient can be calculated by the following equation[22]:

$$(D_K)_A = 9.7 \times 10^3 r(\frac{T}{M_A})^{1/2} \tag{5}$$

where r is the pore radius, nm; $(D_K)_A$ is the Knudsen diffusion coefficient, cm²/s.
The total diffusion coefficient D of the "Dust-Gas" model was calculated by the following equation:

$$D = \frac{1}{1/D_{AB} + 1/(D_K)_A} \tag{6}$$

Given that the catalysts show the single pore size distribution, the effective diffusion coefficient (De) was calculated according to the parallel pore model by the following equation:

$$D_e = \frac{\epsilon D}{\tau} \tag{7}$$

where ε is the porosity, and τ is the curvature factor, which is generally set to 7.

The effectiveness factors were calculated under the typical conditions for the hydrogenation of DMO to MG: P_t=25 atm，T=220 °C，LHSV=1 h⁻¹，H₂/DMO=100，m_{cat}=1.35 g. The corresponding parameters for H₂ and DMO are: σ_{H2}=2.915 nm, σ_{DMO}=5.504 nm, σ_{H_2-DMO}= 4.2095 nm; and the parameters for the pellet catalyst are: porosity = 43%, 5 wt.% Ag/SiO₂. According to the abovementioned conditions, the values for the diffusion coefficient(De) are listed in **Table S7**.

Table S7. Diffusion coefficients of the catalysts

	H	E20	E40	E60	E80
r (nm)	3.90	3.72	3.74	3.81	3.88
D_e (cm²/s)	0.00226	0.00222	0.00223	0.00224	0.00226

Considering that the amount of H_2 is greatly excessive in this reactant, the order of the H_2 was presumably set to be zero. Therefore, the kinetics for DMO hydrogenation in the power-law formula can be written as[23]:

$$r = kC_A^n \tag{8}$$

where C_A is the concentration of DMO.

The internal efficiency factor η[24] is defined as follows:

$$\eta = \frac{Actual\ overal\ rate\ of\ reaction}{Rate\ evaluated\ at\ exterior\ surface\ conditions} \tag{9}$$

Due to the presence of internal diffusion, there is a certain concentration distribution on the inner and outer surfaces of the pellet catalyst, and the actual reaction rates along the pellet are different. An average value of the reaction rate of the whole pellet catalyst was employed for the actual reaction rate as:

$$\bar{r} = \frac{\int_0^{V_p} kc_A^n dV_P}{V_P} \tag{10}$$

where V_P is the particle volume of the catalyst. If the internal diffusion was excluded for the reaction, the reaction rate can be written as kc_{AS}^n, where the concentration of DMO within the pellet catalyst is identical to that outside the pellet atalyst, and thus the effecctiveness factor was calculated as:

$$\eta = \frac{\bar{r}}{kc_{AS}^n} = \frac{\int_0^{V_p} kc_A^n dV_P}{V_P kc_{AS}^n} \tag{11}$$

Before calculating the effectiveness factor under isothermal conditions, the concentration distribution of component DMO within the catalyst particle needs to be determined. Under steady-state conditions, the derivative of the diffusion flux multiplied by the diffusion area with respect to the differential volume is equal to the reaction rate:

$$r = \frac{d(Diffusion\ flux\ \times Diffusion\ area)}{dV_p} = kC_A^n \tag{12}$$

where the diffusion area is given by $4\pi r^2 dr$, and the diffusion flux written as $D_e \frac{dC_A}{dr}$. The equation (9) can be expressed as:

$$De \left(\frac{d^2C_A}{d_r{}^2} + \frac{2dC_A}{r \, dr} \right) = kC_A^n$$

(13)

For the egg-shell-type Ag/SiO$_2$ catalysts tested under excluding the effect of external diffusion, two boundary conditions for equation (13) are given by.

$r = R_0, C_A = C_{As} = C_{A0}$

$r = R_e, C_A = 0.2 \times C_{A0}, (for \, R_e = 0, \frac{dC_A}{dr} = 0)$

Considering that the actual DMO conversion of is greater than or equal to 80% under the set reaction conditions, the DMO conversion is uniformly set to 80% in the calculation. R_0 is the radius of the pellets catalyst and R_e is the starting radius of the catalyst shell layer. Numerical solution for equation (13) was achieved by using MATLAB code. In addition, the formula for the value of k is derived from the relationship between residence time and conversion of DMO as:

$$(1 - x_A)^{1-n} = 1 + (n-1)C_{A0}^{n-1}kt \, , \, n \neq 1$$

(14)

$$1 - x_A = e^{-kt}, n = 1$$

(15)

The formulas for calculating k at different reaction orders are shown as:

$$k = \frac{(1 - x_A)^{1-n} - 1}{(n-1)C_{A0}^{n-1}t}, n \neq 1$$

(16)

$$k = \frac{1}{t}ln\frac{1}{1-x_A}, n = 1$$

(17)

The flow rate of hydrogen is 223.4 ml/min here, and the catalyst bed is a cylinder with a bottom diameter of 3.2 cm and a height of 2.5 mm, based on which the residence time was estimated according to the following equation:

$$t = \frac{V_{cylinder}}{H_2 \, flow \, rate} = \frac{1.6^2 \times \pi \times 0.25}{223.4} \times 60 = 0.54s$$

Under the conditions of H$_2$/DMO=100 (mol/mol), P=25 atm, T=493 K, and H$_2$ flow rate of 223.4 ml/min, C_{A0} was estimated to 6.039 $\times$ 10^{-3} mol/L according to the ideal gas equation of state. Based on these parameters, the values of k were calculated by specifying the reaction orders of DMO at different levels and shown in **Table S8**. According to the calculated values for k, De and the corresponding boundary conditions for Eq. (10), the numerical solution of the concentration distribution at a specific reaction order of DMO (n) can be obtained, and then the effectiveness factor (η) can be calculated by equation (8). The calculated values for the effectiveness factor under different specific reaction order of DMO are listed in **Table S9**.

Table S8. Calculated values of k by specifying different reaction orders for DMO.

Reaction order of DMO	0.5	1	1.5	2

k	0.1591	2.9800	58.9110	1226.5950

Table S9. Calculated values for effectiveness factor (η) for the catalysts by specifying different reaction orders for DMO.

	n=0.5	n=1	n=1.5	n=2
E20	0.7725	0.6135	0.4929	0.3946
E40	0.7413	0.5680	0.4361	0.3308
E60	0.7104	0.5382	0.4093	0.3075
E80	0.6896	0.5234	0.3983	0.2990
H	0.6730	0.5157	0.3942	0.2966
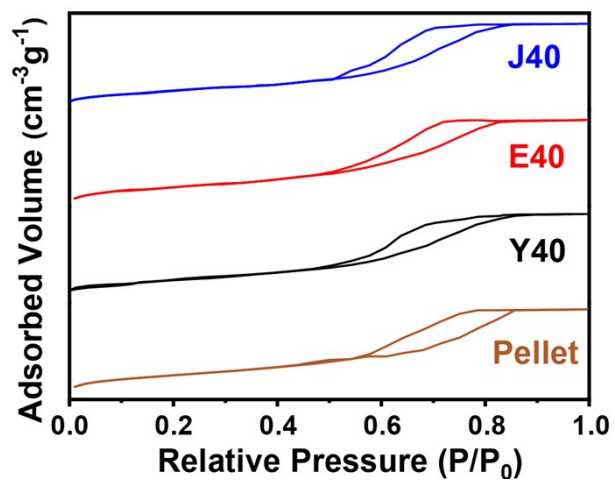
Fig. S1. N_2 physical adsorption-desorption isotherms of J40, E40 and Y40 catalysts as well as the SiO$_2$ pellet.
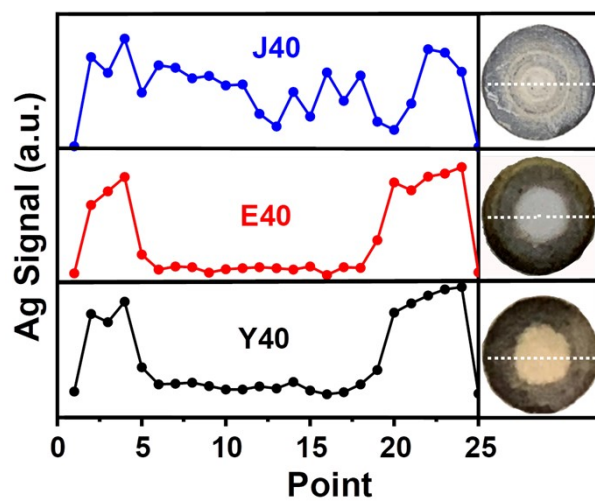
Fig. S2. SEM-EDX line-scanning profiles for the half-sliced J40, E40, and Y40 catalysts to demonstrate the Ag distributions.
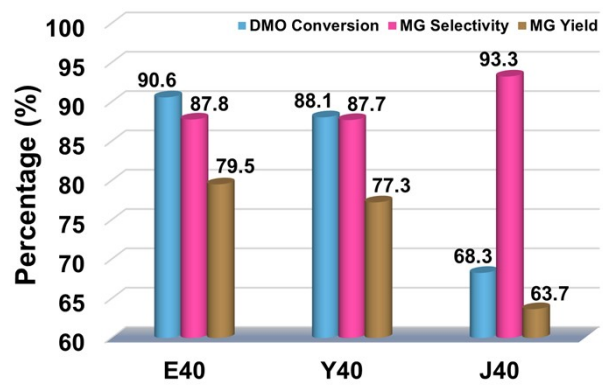
Fig. S3. Comparison for the DMO conversion, MG selectivity and MG yield of the three catalysts prepared with different hydrophobic solvents at the LHSV of 1 h^{-1}.
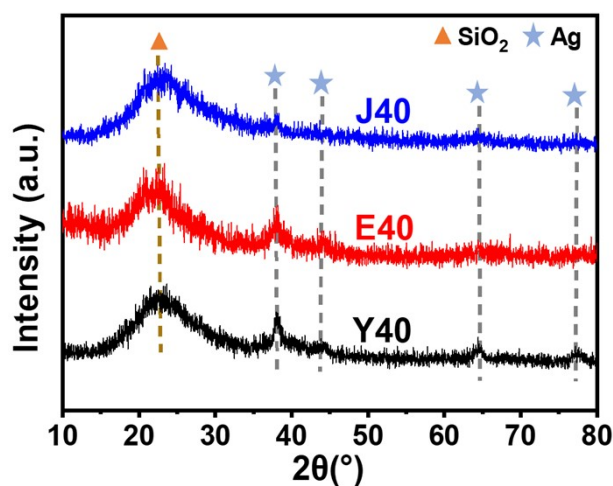
Fig. S4. XRD patterns of J40, E40 and Y40 catalysts.

Notes: As seen in Fig. S1, the as-prepared catalysts exhibit similar pore structures, which are similar to that of SiO_2 pellet. The scanning electron microscope (SEM) images of these three catalysts clearly indicate the egg-shell structures, except the J40 catalyst (Fig. S2). Moreover, the SEM energy dispersive X-ray diffraction (SEM-EDX) line-scanning profiles show the distribution of Ag in the shell of E40 and Y40 catalysts, and the thickness of Ag-shell is determined to be close for these two catalysts. However, the catalytic performances of the E40 catalyst is superior to those of the Y40 in the terms of DMO conversion and MG yield (Fig. S3). The preferable performance of the E40 catalyst over that of the Y40 catalyst could be assigned to the better dispersion of Ag in the E40 catalyst, as revealed by the weaker intensities of diffraction peaks corresponded to Ag in XRD pattern of E40 (Fig. S4).
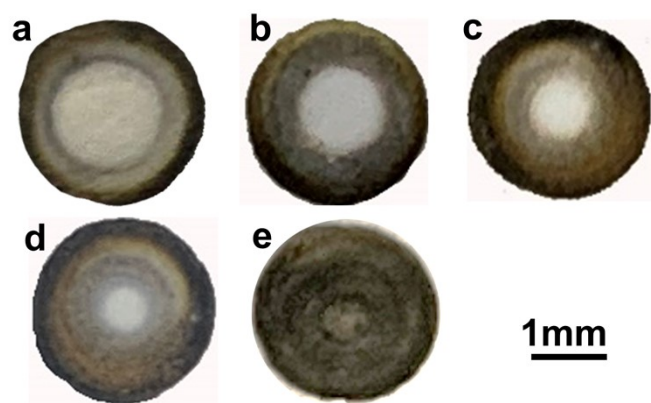
Fig. S5. Typical photos of the half-sliced of Ag-shell of (a) E20, (b) E40, (c) E60, (d) E80 and (e) H catalysts. (Scale bar: 1 mm)
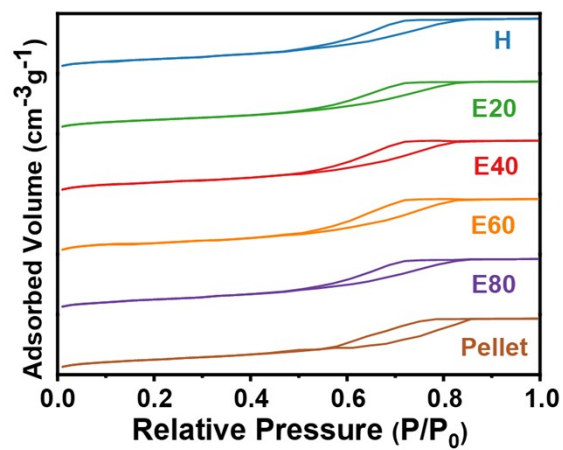
Fig. S6. N$_2$ adsorption–desorption isotherms of the H, E20, E40, E60 and E80 catalysts as well as the SiO$_2$ pellet.
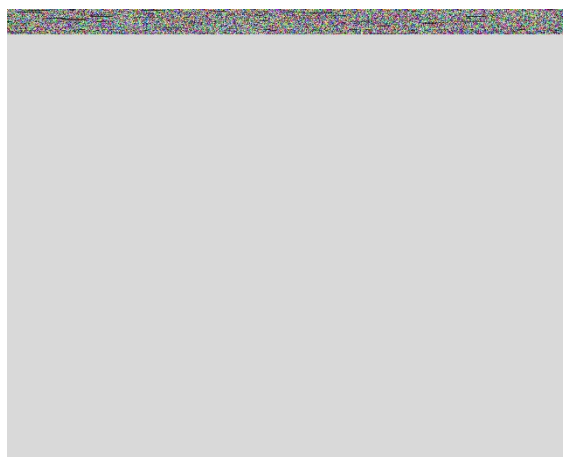
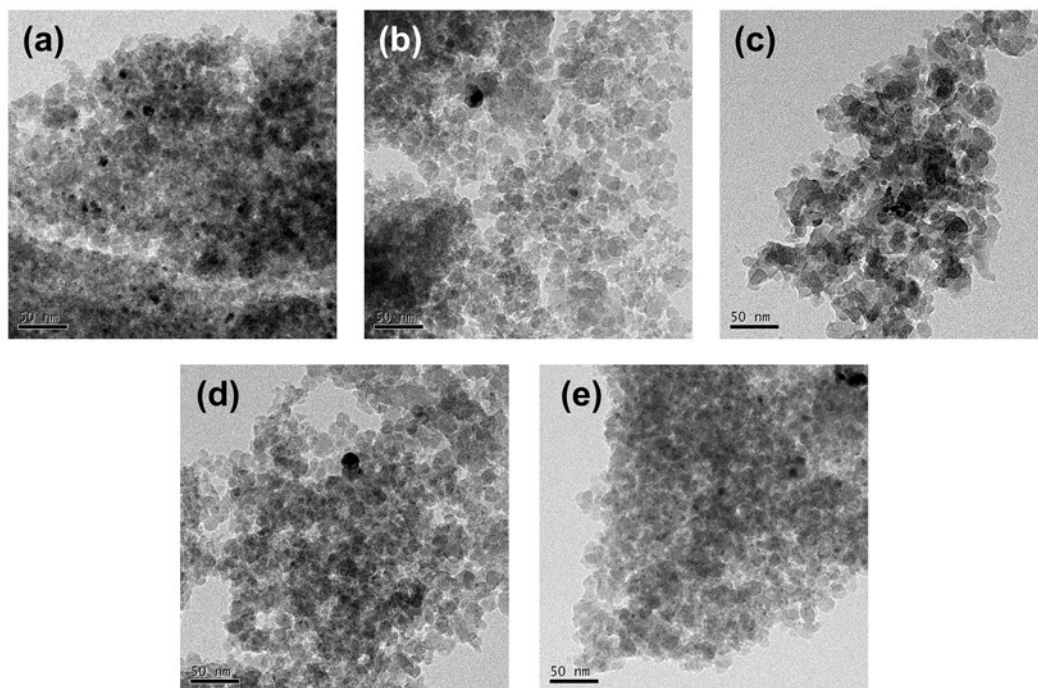**Fig. S7.** Pore size distributions of the H, E20, E40, E60 and E80 catalysts as well as the SiO$_2$ pellet.

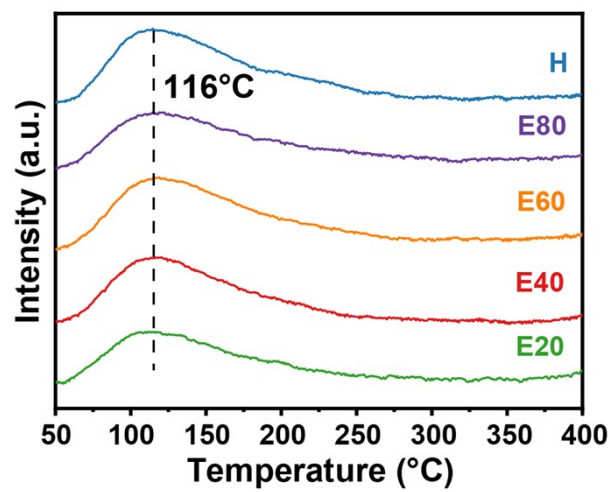**Fig. S8.** Typical TEM images of Ag-shell of (a) E20, (b) E40, (c) E60, (d) E80 and (e) H catalysts.

Fig. S9 H$_2$-TPD profiles of Ag/SiO$_2$ egg-shell catalysts and the H catalyst.
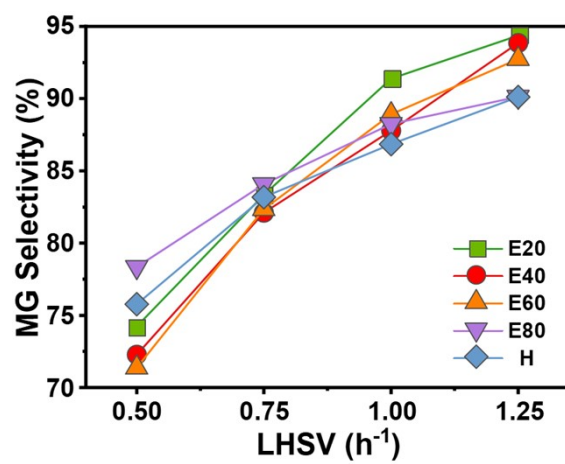
Fig. S10 MG selectivity as a function of LHSV over the Ag/SiO2 egg-shell catalysts and the H catalyst.
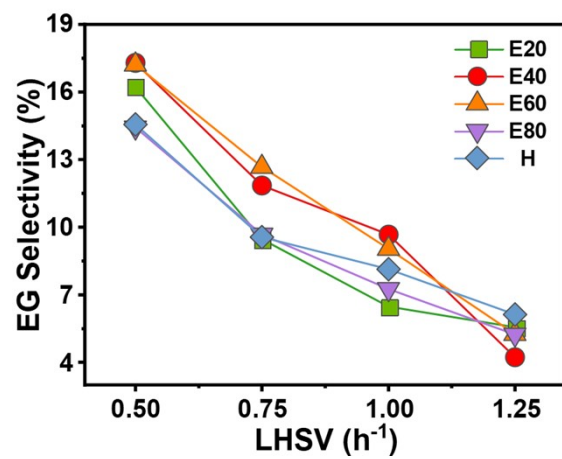
Fig. S11 EG selectivity as a function of LHSV over the Ag/SiO2 egg-shell catalysts and the H catalyst.

Reference

1. G. Dong, Y. Cao, S. Zheng, J. Zhou, W. Li, F. Zaera and X. Zhou, *J. Catal.*, 2020, **391**, 155-162.
2. Z. Luo, X. Xu, G. Dong, Y. Cao, S. Hu, G. Ye, Y.-A. Zhu, J. Zhou, W. Li and X. Zhou, *Chem. Eng. J.*, 2022, **450**, 138397.
3. J. R. Anderson, *Structure of metallic catalysts*, Academic Press, London ;, 1975.
4. J. Zhou, X. Duan, L. Ye, J. Zheng, M. M.-J. Li, S. C. E. Tsang and Y. Yuan, *Applied Catalysis A: General*, 2015, **505**, 344-353.
5. A. Yin, C. Wen, X. Guo, W.-L. Dai and K. Fan, *J. Catal.*, 2011, **280**, 77-88.
6. X. Kong, C. Ma, J. Zhang, J. Sun, J. Chen and K. Liu, *Applied Catalysis A: General*, 2016, **509**, 153-160.
7. C. Wen, Y. Cui, X. Chen, B. Zong and W.-L. Dai, *Applied Catalysis B: Environmental*, 2015, **162**, 483-493.
8. Y. Cui, B. Wang, C. Wen, X. Chen and W.-L. Dai, *ChemCatChem*, 2016, **8**, 527-531.
9. M. Abbas, Z. Chen, J. Zhang and J. Chen, *New J. Chem.*, 2018, **42**, 10290-10299.
10. Y. Chen, L. Han, J. Zhu, P. Chen, S. Fan, G. Zhao, Y. Liu and Y. Lu, *Catal. Commun.*, 2017, **96**, 58-62.
11. M. Ouyang, J. Wang, B. Peng, Y. Zhao, S. Wang and X. Ma, *Appl. Surf. Sci.*, 2019, **466**, 592-600.
12. H. Chen, J. Tan, J. Cui, X. Yang, H. Zheng, Y. Zhu and Y. Li, *Molecular Catalysis*, 2017, **433**, 346-353.
13. M. Hu, Y. Yan, X. Duan, L. Ye, J. Zhou, H. Lin and Y. Yuan, *Catal. Commun.*, 2017, **100**, 148-152.
14. J. Zheng, X. Duan, H. Lin, Z. Gu, H. Fang, J. Li and Y. Yuan, *Nanoscale*, 2016, **8**, 5959-5967.
15. M. M.-J. Li, L. Ye, J. Zheng, H. Fang, A. Kroner, Y. Yuan and S. C. E. Tsang, *Chem. Commun. (Cambridge, U. K.)*, 2016, **52**, 2569-2572.
16. M. Ouyang, Y. Wang, J. Zhang, Y. Zhao, S. Wang and X. Ma, *RSC Advances*, 2016, **6**, 12788-12791.
17. J. Zheng, H. Lin, X. Zheng, X. Duan and Y. Yuan, *Catal. Commun.*, 2013, **40**, 129-133.
18. A. Yin, C. Wen, W.-L. Dai and K. Fan, *Applied Catalysis B: Environmental*, 2011, **108-109**, 90-99.
19. M. Knudsen, *Annalen der Physik*, 1909, **333**, 75-130.
20. D. M. Ruthven, W. J. DeSisto and S. Higgins, *Chem. Eng. Sci.*, 2009, **64**, 3201-3203.
21. S. Langenberg, T. Carstens, D. Hupperich, S. Schweighoefer and U. Schurath, *Atmos. Chem. Phys.*, 2020, **20**, 3669-3682.
22. S. Li, in *Reaction Engineering*, ed. S. Li, Butterworth-Heinemann, Boston, 2017, DOI: https://doi.org/10.1016/B978-0-12-410416-7.00006-9, pp. 265-310.
23. J. Burés, *Top. Catal.*, 2017, **60**, 631-633.
24. A. K. Avci and Z. I. Önsan, in *Comprehensive Energy Systems*, ed. I. Dincer, Elsevier, Oxford, 2018, DOI: https://doi.org/10.1016/B978-0-12-809597-3.00235-2, pp. 475-523.